Fabrication of ultrahigh aspect ratio freestanding gratings on silicon-on-insulator wafers

Minseung Ahn,[a] Ralf K. Heilmann, and Mark L. Schattenburg
Massachusetts Institute of Technology, Cambridge, Massachusetts 02139

(Received 6 June 2007; accepted 23 July 2007; published 11 December 2007)

The authors report a silicon-on-insulator (SOI) process for the fabrication of ultrahigh aspect ratio freestanding gratings for high efficiency x-ray and extreme ultraviolet spectroscopy. This new grating design will lead to blazed transmission gratings via total external reflection on the grating sidewalls for x rays incident at graze angles below their critical angle (about 1°–2°). This critical-angle transmission (CAT) grating combines the alignment and figure insensitivity of transmission gratings with high broadband diffraction efficiency, which traditionally has been the domain of blazed reflection gratings. The required straight and ultrahigh aspect ratio freestanding structures are achieved by anisotropic etching of ⟨110⟩ SOI wafers in potassium hydroxide (KOH) solution. To overcome structural weakness, chromium is patterned as a reactive ion etch mask to form a support mesh. The grating with period of 574 nm is written by scanning-beam interference lithography (SBIL) which is based on the interference of phase-locked laser beams. Freestanding structures are accomplished by etching the handle and device layers in tetramethylammonium hydroxide and KOH solution, respectively, followed by hydrofluoric acid etching of the buried oxide. To prevent collapse of the high aspect ratio structures caused by water surface tension during drying, the authors use a supercritical point dryer after dehydration of the sample in pure ethanol. The authors have successfully fabricated 574 nm period freestanding gratings with support mesh periods of 70, 90, and 120 μm in a 10 μm thick membrane on ⟨110⟩ SOI wafers. The size of a single die is 10×12 mm^2 divided into four 3×3.25 mm^2 windows. The aspect ratio of a single grating bar achieved is about 150, as required for the CAT grating configuration. © *2007 American Vacuum Society.* [DOI: 10.1116/1.2779048]

I. INTRODUCTION

Diffraction gratings have been used by x-ray astronomers to reveal an invisible universe above the atmosphere which absorbs incoming x rays.[1–3] The Chandra Observatory, launched in 1999, is equipped with a high energy transmission grating spectrometer consisting of 200 and 400 nm period gold transmission gratings.[2–5] Although transmission gratings have played a useful role in x-ray spectroscopy, their peak diffraction efficiency is generally lower than that of blazed grazing-incidence reflection gratings.[6] Reflection gratings,[7,8] on the other hand, have high sensitivity to alignment and surface figure and much higher mass, which is not desirable in space instrumentation. Combining the advantages of these two grating types, we designed a novel transmission grating that has grating bars with ultrahigh aspect ratio (height/width) and extremely smooth sidewalls. In a transmission grating configuration, x rays incident at small graze angles are specularly reflected from the smooth sidewalls, which leads to a blazing effect and high diffraction efficiency. Figure 1(a) shows the basic concept and working configuration. Due to the small critical angles for soft x rays ($\sim 1°-2°$), very high aspect ratio grating bars are required. The sidewalls roughness should be less than 1 nm for maximum reflectivity. In addition, the grating has to be freestanding to minimize soft x-ray absorption, and the period should be on the order of 100 nm to diffract nanometer wavelength x rays with high enough dispersion.

We designed a ⟨110⟩ silicon-on-insulator (SOI) process to address the challenging fabrication issues for a critical-angle transmission (CAT) grating prototype. Vertical and smooth grating bar sidewalls can be accomplished by utilizing anisotropic KOH etching. Silicon etch rates in KOH solution depend on the crystal orientation. For example, the etch rate of ⟨110⟩ is known to be orders of magnitude faster than that of the ⟨111⟩ direction.[9–13] In addition, the {111} planes can be atomically smooth and act as a mirrorlike surface.[7,8] Therefore, a vertical and smooth etch profile can be attained by aligning the grating pattern with the {111} planes in the ⟨110⟩ wafer surface. Figure 2 shows the ⟨110⟩ wafer's cleavage angles and the anisotropic etch profile. There are six {111} planes: two pairs of vertical planes and two slanted planes. The slanted {111} planes limit the maximum etch depth $D_{\max}$ to $L/2\sqrt{3}$.[10,11] Therefore, the open gap width between the bars of the support mesh must be wide enough for the fine grating to be etched through to the required thickness. A freestanding structure can be attained by etching both sides of a SOI wafer, followed by etching the buried oxide.

In the following, we will describe the fabrication steps in detail and demonstrate a CAT grating prototype with a relatively large period (574 nm) on wafers with a 10 μm thick SOI layer.

[a]Electronic mail: msahn@mit.edu

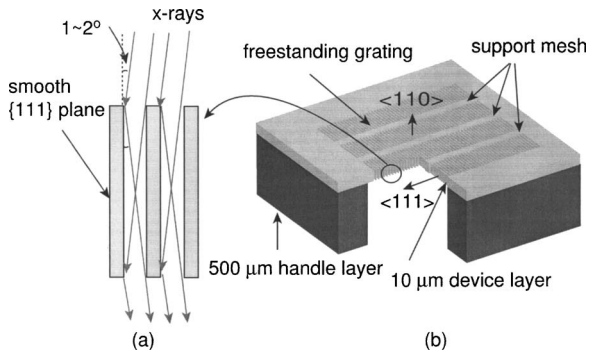

FIG. 1. (a) Concept of the critical angle transmission (CAT) grating. The incoming x rays have a small graze angle so that they will be strongly diffracted in the specular reflection direction due to total external reflection on the smooth sidewalls. (b) Schematic design for the CAT grating prototype utilizing ⟨110⟩ single crystal silicon, which can be etched with vertical and atomically smooth {111} sidewalls.

II. FABRICATION PROCESS

A. Patterning process

Our substrates were 100 mm diameter ⟨110⟩ SOI wafers (Ultrasil, CA) with a 10 ± 0.5 μm device layer, 2 ± 0.1 μm buried oxide, and 500 μm handle layer. The wafer has two flats in the ⟨111⟩ directions with ±0.2° tolerance. The etch profile of ⟨110⟩-oriented silicon with a parallelogram mask is shown in Fig. 2(b). The vertical sidewalls are atomically smooth {111} planes with which the grating bars are supposed to be aligned. The thermally grown buried oxide will act as an etch stop for the anisotropic etch of the handle layer

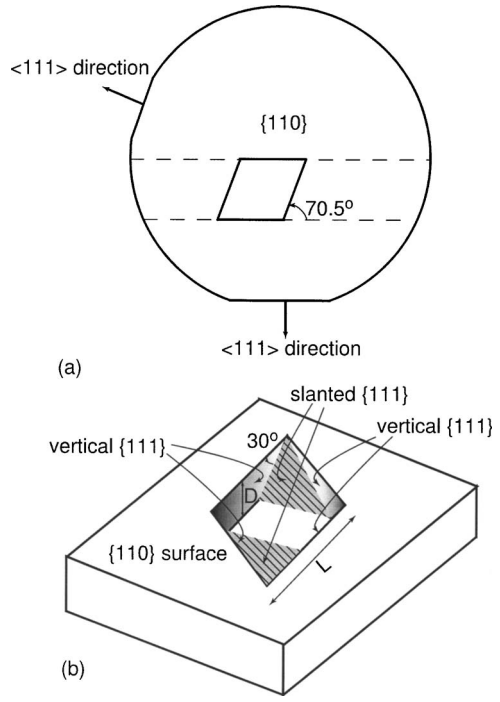

FIG. 2. (a) ⟨110⟩ silicon wafer's flat orientations and cleavage parallelogram along the {111} planes. (b) Anisotropic etch profile of ⟨110⟩ silicon consisting of two pairs of vertical {111} planes and one pair of 35.26° tilted {111} planes from the (110) top surface. The projection of the slanted {111} planes onto the vertical {111} has an angle of 30° from the (110) top surface.

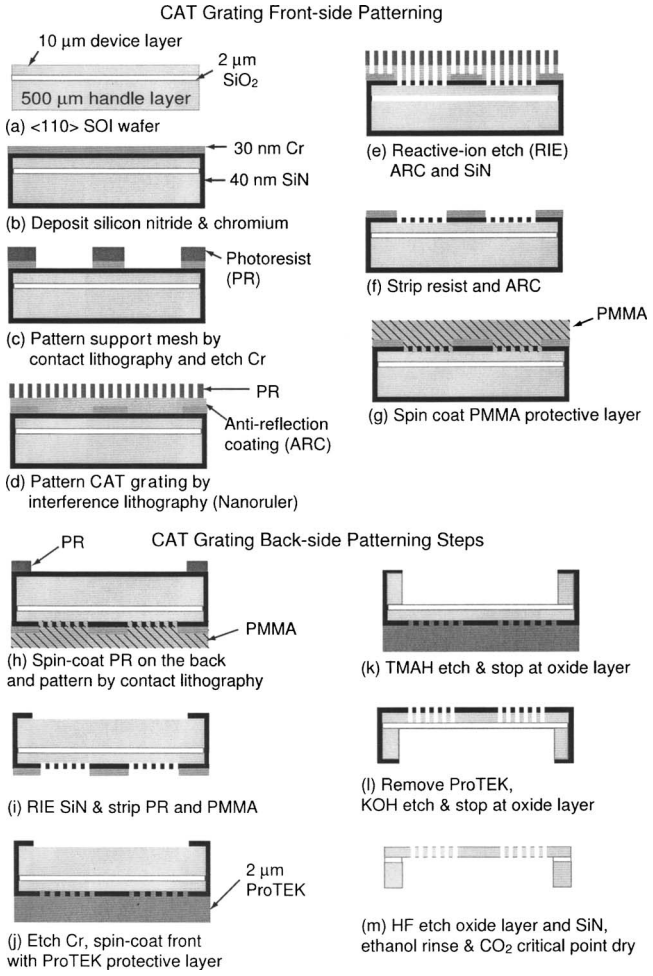

FIG. 3. CAT grating fabrication process; [(a)–(g)] front-side patterning to form SiN mask of the grating and support mesh, [(h)–(k)] back side patterning to form the membrane and frame, and [(l) and (m)] KOH etching, HF etching, and supercritical point drying to form the high aspect ratio freestanding grating.

from the back side. A thin (40 nm) silicon-rich nitride layer was deposited on the substrate by low pressure chemical vapor deposition to serve as a wet etch mask. Using an electron beam evaporator, 30 nm of chromium was deposited as a reactive ion etch mask to form the support mesh [Fig. 3(b)].

The Cr layer was patterned by contact lithography and wet etching in perchloric acid CR-7 (Cyantek, CA) [Fig. 3(c)]. We patterned support structures with 70, 90, and 120 μm pitches and a wide cross which was aligned with the cross pattern on the back side to divide the large (10×12 mm^2) area of the membrane into four parts. Figure 4(a) shows an etched Cr reactive ion etching (RIE) mask pattern with a 70 μm pitch.

On top of the support mesh, 110 nm of antireflection coating (ARC) (XHRiC-11, Brewer Science Inc.) and 700 nm of photoresist (PFI-88a7, Sumitomo Corp.) were spin coated for interference lithography. The fine period (574 nm) grating was written by scanning-beam interference lithography[14,15] (SBIL) which is based on the interference of phase-locked millimeter-sized laser beams of 351 nm wavelength [Figs.

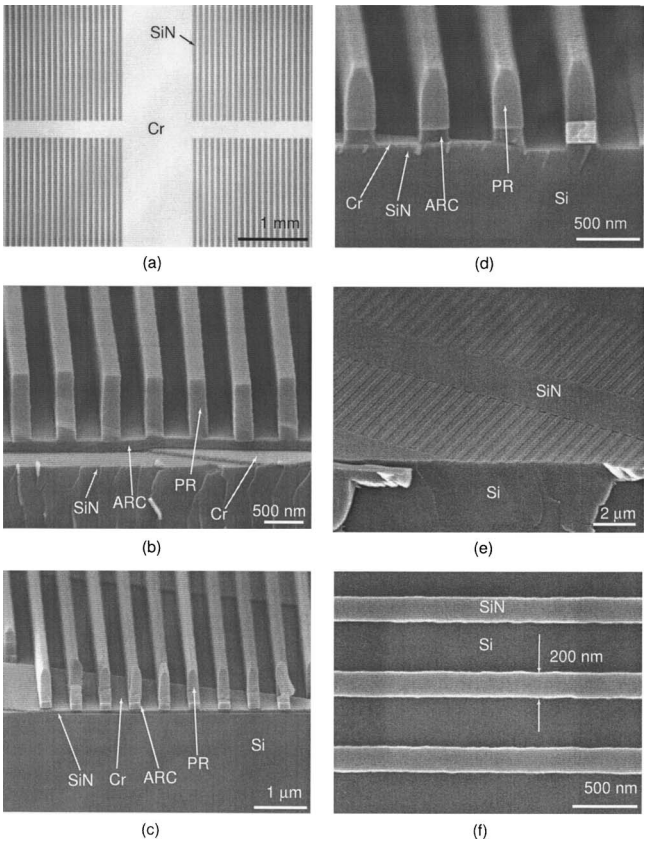

FIG. 4. Micrographs of the patterning steps. (a) Cr support mesh pattern with 70 μm period on the SiN layer. (b) Photoresist pattern of the fine grating after scanning-beam interference lithography. (c) Pattern transferred to ARC. (d) Pattern transferred to SiN. (e) SiN pattern of the fine grating and the support mesh after removing PR, ARC, and Cr. (f) Top view of SiN fine grating lines between 70 μm period support meshes on a SOI wafer to be etched in the KOH solution. Note that (b)–(d) are taken from a ⟨100⟩ test wafer with narrow support mesh (period=7 μm) to show the support meshes and the fine grating in a single image.

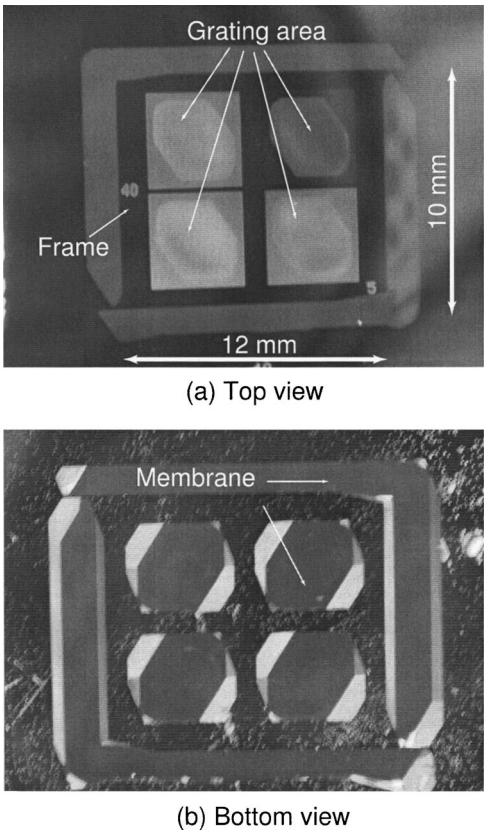

FIG. 5. Photographs of one grating unit after TMAH etching. The bright parts in (a), including four grating areas and the outer frame boundary, are the membranes of 10 μm of Si and 2 μm of SiO_2 etched from the back. The grating areas, except for the top right quadrant, are brighter due to diffraction from the SiN grating. The top right quadrant has only the support mesh pattern for test purposes.

3(d) and 4(b)]. The interference fringe direction was aligned with the wafer flat to within ±0.1° using a microscope mounted on the vertical optical bench of the SBIL system looking down on the wafer flat. The wafer flat was aligned to have a fixed position in the microscope when moving the scanning stage along the fringe direction. The grating pattern in the photoresist was developed and transferred into the ARC and silicon nitride with RIE. The ARC was etched using O_2 plasma and the silicon nitride etched using $CF_4 + O_2$ plasma [Figs. 3(e), 4(c), and 4(d)]. A RCA clean (hydrogen peroxide: ammonia hydroxide: water, 1:1:5) removed the photoresist and ARC [Fig. 3(f)]. The front side was then spin coated with polymethyl methacrylate (PMMA) or thick photoresist to protect the front pattern during the following back side patterning process [Fig. 3(g)].

The back side was patterned by contact lithography and RIE to serve as a hard mask for tetramethylammonium hydroxide (TMAH) etching to form a thin membrane [Figs. 3(h) and 3(i)]. The pattern is a simple window shape with a 12×10 mm^2 outer release frame and cross in the middle. After removing the photoresist, PMMA, and Cr, the wafer is ready for anisotropic wet etching [Fig. 4(e)]. The fine nitride grating linewidth was about 200 nm, as shown in Fig. 4(f).

B. Anisotropic wet etching

In order to cover the front side pattern during the back side TMAH etching, 2 μm of protective layer with a primer (ProTEK, Brewer Science Inc.) was spin coated on top of the device layer [Fig. 3(j)]. Because the selectivity between Si and SiO_2 in TMAH solutions is very high,[11] the buried oxide is a good etch stop. The etch rate for the (110) plane was about 1.4 μm/min in 25% TMAH at 90 °C. Figure 5 shows top and bottom views of a single device after TMAH etching. We can see through the thin (10 μm) silicon layer which is partially transparent with a red color. Three quadrants of the device have the fine grating with support mesh, but the top right quadrant has support structure only for test purposes. The back side nitride mask had a square window shape, but the etched profile in Fig. 5(b) shows etch anisotropy in TMAH solution. The width of the outer frame and the central cross masking were designed to be wide enough to account for the expected undercut. The thin bridges at the corners prevent the device from detaching during wet processing. The silicon membranes tend to buckle slightly due to the compressive stress of the buried oxide layer, but flatten

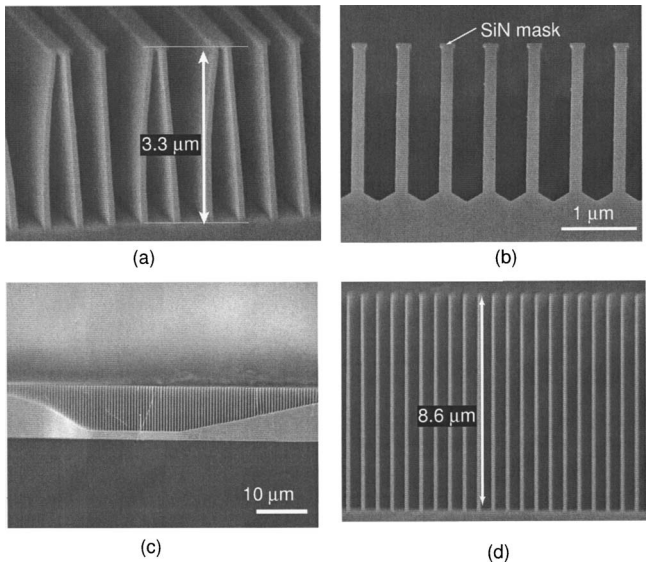

FIG. 6. Electron micrographs after KOH etching. (a) Etched for 1.5 min in 40 wt % KOH with isopropyl alcohol (IPA) at 80 °C and dried in air. Alcohol addition made the etch front flat, but reduced the anisotropy. Air drying caused a stiction problem. (b) Etched for 1 min in 45 wt % KOH at 80 °C and dried in air. There is considerable lateral etching (undercut). (c) Cross-sectional view of a slightly underetched sample in 50 wt % KOH at 60 °C and dried by a supercritical point dryer. (d) Close view of (c). A low temperature in a high KOH concentration produced a flat etch front, as compared to (b).

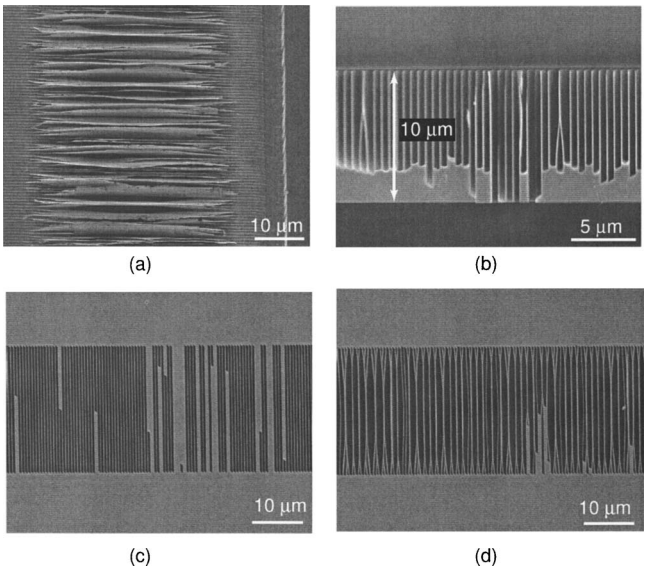

FIG. 7. Electron micrographs of KOH etching problems. (a) Top view of an overetched sample due to the low anisotropy in 45 wt % KOH at 80 °C. The grating bars were thinned and the nitride mask was lost during etching. (b) Cross-sectional view of a sample with nonuniform etching. (c) Bottom view of a sample with nonuniform etching. (d) Bottom view of a sample with stiction in spite of supercritical point drying. (b)–(d) were etched in 50 wt % at 50 °C.

at the end of the process after HF etching. We found no evidence of the stress causing any problem during the KOH etch.

After removing the ProTEK with solvent and a short oxygen plasma etch, the grating was anisotropically etched in 50 wt % KOH/water solution at 50 °C for 55 min to etch through the 10 μm silicon [Fig. 3(l)]. The loss of the nitride mask and buried oxide is expected to be less than 1 and 25 nm, respectively.[9,11] KOH etching is the most challenging process step because the anisotropy or etch rate ratio is very sensitive to temperature, KOH concentration, additives, and so forth. We will discuss these variances in the next section. After KOH etching, the buried oxide and nitride mask were removed by a 5 min etch in concentrated (48%) HF.

Because of the high aspect ratio and rinse water surface tension, drying in air leads to sticking problems. Figure 6(a) shows stiction after air drying even though the aspect ratio of a grating bar is only about 20. Considering our goal aspect ratio of 150, we instead used a liquid carbon dioxide supercritical point dryer (Tousimis, MD) after dehydration with pure ethanol [Fig. 3(m)]. Figures 6(c) and 6(d) show that the stiction problem was solved by supercritical point drying. Special care had to be taken during transfer of the sample in order to prevent drying.

III. RESULTS AND DISCUSSION

First attempts to etch through the 10 μm silicon device layer resulted in only partial success or totally destroyed grating lines [Fig. 7(a)] due to insufficient etch anisotropy and overetching in 45 wt % KOH at a high temperature (80 °C), although Kendall[10] achieved an anisotropy of 600 under similar etching conditions. In order to understand that etching condition, a 1 min KOH etch was performed in 45 wt % KOH at 80 °C. The etch profile is shown in Fig. 6(b). The vertical etch rate (R_{110}) was 1.86 μm/min and the lateral etch rate (R_{111}) was 26 nm/min. The anisotropy ratio, R_{110}/R_{111}, is about 70, which is much lower than that reported in previous literature.[10–13] One explanation might be misalignment between the grating pattern and the crystal direction. However, Krause and Obermeier[16] also showed an anisotropy dependence on the groove width. An anisotropy of 70 for our 0.37 μm groove width agrees well with their experimental behavior. In any case, given the nitride linewidth of 0.2 μm [Fig. 4(f)] and the low anisotropy in the 80 °C etching condition above, the grating bars will thin away and the silicon nitride mask will detach before the oxide etch stop is reached.

Kim *et al.*[17] and Hölke and Henderson[12] reported an increase in the etch rate ratio in high KOH concentrations and at low temperatures. With 50 wt % KOH at 50 °C, we achieved an improved anisotropy ratio of about 125. While an apex formed at the etch front in a high concentration at a high temperature, as shown in Fig. 6(b), with an alcohol additive or at a low temperature below 60 °C, the shape of the etch front changed to a flat, as shown in Figs. 6(a) and 6(d). Once an apex is formed, the vertical etch rate decreases and thus the anisotropy degrades. However, although a sufficient anisotropy was achieved, etching was not uniform over the whole grating area, as shown Fig. 7(b). Stirring with a magnet bar and ultrasonic agitation did not help much, or resulted in unfavorable damage to the membrane, as Kaminsky[13] has observed. Because KOH etching produces

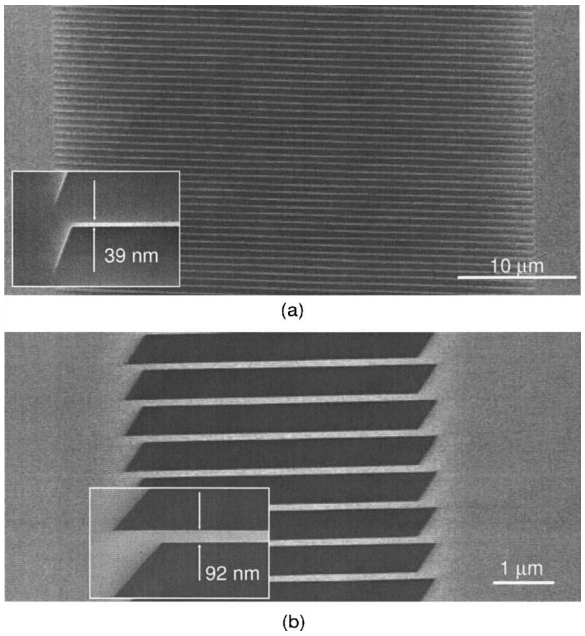

FIG. 8. Electron micrographs of a CAT grating between the support mesh bars. (a) Top view of the fine grating between a 40 μm open gap. The linewidth at the top is 39 nm. (b) Bottom view of the grating. The open gap is shrunk to ~5 μm to due the slanted {111} planes. The linewidth is 92 nm, which is consistent with an average sidewall slope of ~0.15°.

an abundance of H_2 bubbles, trapping of bubbles between the grating bars might intermittently interfere with the reaction. Samples immersed horizontally (facing upward) resulted in better uniformity than those immersed vertically [compare Fig. 6(d) with 7(b)]. Facing the fine grating bars upward might reduce trapping of H_2 bubbles.

With 50 wt % KOH at 50 °C, we achieved ultrahigh aspect ratio freestanding transmission gratings. Figure 8 shows top and bottom views of a freestanding grating with a 70 μm pitch support structure. The open gap between support lines was 40 μm at the top and 5 μm at the bottom, which agrees well with the crystal angle, as shown in Fig. 2(b). The linewidths of a single grating bar are ~40 nm at the top and ~90 nm at the bottom. The aspect ratio of the grating bar is 152 based on the average width of 65 nm. The slope angle of the sidewalls is only about 0.15°. The sidewall roughness (root mean square) of a test sample is less than 0.2 nm over 65×65 nm^2 area, which was measured by an atomic force microscope.

For wider support mesh periods of 90 and 120 μm, similar results were obtained in some areas. However, there are still occasional uniformity and stiction problems, as shown in Figs. 7(c) and 7(d). One potential solution is to find the actual ⟨111⟩ direction using a pre-etch technique, as described in Ref. 9, for better pattern alignment to the crystal. By etching the wafer anisotropically with a fan-shaped masking pattern, the ⟨111⟩ crystal direction can be determined accurately to within ±0.05°. Various surfactants that reduce the surface tension and increase the wetting ability without significantly changing the anisotropy may also improve uniformity. Generally, alcohol additives are not preferred for high aspect ratio etching because alcohols slow down the etch rate of ⟨110⟩ and degrade the anisotropy.[10] However, an anionic surfactant (e.g., dihexyl ester of sodium sulfosuccinic acid) has been shown to reduce the contact angle to a half of the pure 30 wt % KOH solution.[18]

IV. CONCLUSION AND FUTURE WORK

We have developed and demonstrated a bulk micromachining process for the fabrication of ultrahigh aspect ratio freestanding gratings on SOI wafers. An aspect ratio of 150 was achieved by using high concentration KOH etching at a low temperature, followed by supercritical point drying. Freestanding single grating bars are 10 μm tall, ~40 nm wide at the top, and ~90 nm wide at the bottom with 0.15° sidewall slopes. This prototype grating will be tested with soft x rays to demonstrate the blazing effect and to determine its diffraction efficiency.

Although the support structures are important to reinforce the freestanding gratings, their area should be minimized to increase x-ray throughput. We plan to improve the etch uniformity and repeatability of support gratings with periods of 90 and 120 μm on the device layer, and will work to optimize the support structures and the fabrication process. With a reliable fabrication process, our next goal is to develop 200 nm period freestanding gratings with similar aspect ratios.

ACKNOWLEDGMENTS

The authors gratefully acknowledge the assistance of Robert Fleming of the MIT Space Nanotechnology Laboratory and James Daley of the MIT NanoStructures Laboratory. They thank Nicki Watson and Erika Batchelder for help with the supercritical point dryer at the MIT Whitehead Institute and the MIT Microsystems Technology Laboratories for facility support. This work was supported by NASA Grant No. NNG05WC13G and a Samsung Scholarship.

[1] M. L. Schattenburg *et al.*, Opt. Eng. (Bellingham) **30**, 1590 (1991).
[2] M. L. Schattenburg, J. Vac. Sci. Technol. B **19**, 2319 (2001).
[3] M. C. Weisskopf, Proc. SPIE **5488**, 25 (2004).
[4] T. H. Markert, C. R. Canizares, D. Dewey, M. McGuirk, C. S. Pak, and M. L. Schattenburg, Proc. SPIE **2280**, 168 (1994).
[5] C. R. Canizares *et al.*, Publ. Astron. Soc. Pac. **117**, 1144 (2005).
[6] M. C. Hettrick, M. E. Cuneo, J. L. Porter, L. E. Ruggles, W. W. Simpson, M. F. Vargas, and D. F. Wenger, Appl. Opt. **43**, 3772 (2004).
[7] A. E. Franke, M. L. Schattenburg, E. M. Gullikson, J. Cottam, S. M. Kahn, and A. Rasmussen, J. Vac. Sci. Technol. B **15**, 2940 (1997).
[8] C.-H. Chang *et al.*, J. Vac. Sci. Technol. B **22**, 3260 (2004).
[9] H. Seidel, L. Csepregi, A. Heuberger, and H. Baumgartel, J. Electrochem. Soc. **137**, 3626 (1990).
[10] D. L. Kendall, Annu. Rev. Mater. Sci. **9**, 373 (1979).
[11] M. J. Madou, *Fundamentals of Microfabrication, The Science of Miniaturization*, 2nd ed. (CRC, Boca Raton, FL, 2002), pp. 212–220.
[12] A. Hölke and H. Henderson, J. Micromech. Microeng. **9**, 51 (1999).
[13] G. Kaminsky, J. Vac. Sci. Technol. B **3**, 1015 (1985).
[14] P. T. Konkola, C. G. Chen, R. K. Heilmann, C. Joo, J. C. Montoya, C.-H. Chang, and M. L. Schattenburg, J. Vac. Sci. Technol. B **21**, 3097 (2003).
[15] R. K. Heilmann, C. G. Chen, P. T. Konkola, and M. L. Schattenburg, Nanotechnology **15**, S504 (2004).
[16] P. Krause and E. Obermeier, J. Micromech. Microeng. **5**, 112 (1995).
[17] S.-H. Kim, S.-H. Lee, H.-T. Lim, Y.-K. Kim, and S.-K. Lee, in *Sixth International Connference on Emerging Technologies and Factory Automation Proceedings* (IEEE, Los Angeles, CA, 1997), pp. 248–252.
[18] C.-R. Yang, P.-Y. Chen, Y.-C. Chiou, and R.-T. Lee, Sens. Actuators, A **119**, 263 (2005).